Chitosugar translocation by an unexpressed monomeric protein channel

H. Sasimali M. Soysa and Wipa Suginta
Biochemistry-Electrochemistry Research Unit, School of Chemistry, Institute of Science, Center of Excellence in Advanced Functional Materials, Suranaree University of Technology, Nakhon Ratchasima 30000, Thailand

Watcharaporn Moonsap and M. F. Smith
School of Physics, Institute of Science, Suranaree University of Technology, Nakhon Ratchasima 30000, Thailand

(Received 26 December 2017; revised manuscript received 24 March 2018; published 31 May 2018)

The outer membrane protein channel *Ec*ChiP, associated with a silent gene in *E. coli*, is a monomeric chitoporin. In a glucose-deficient environment, *E. coli* can express the ChiP gene to exploit chitin degradation products. Single-channel small ion current measurements, which reveal the dynamics of single sugar molecules trapped in channel, are used here to study the exotic transport of chitosugars by *E. coli*. Molecules escape from the channel on multiple timescales. Voltage-dependent trapping rates observed for charged chitosan molecules, as well as model calculations, indicate that the rapid escape processes are those in which the molecule escapes back to the side of the membrane from which it originated. The probability that a sugar molecule is translocated through the membrane is thus estimated from the current data and the dependence of this translocation probability on the length of the chitosugar molecule and the applied voltage analyzed. The described method for obtaining the translocation probability and related molecular translocation current is applicable to other transport channels.

DOI: 10.1103/PhysRevE.97.052417

I. INTRODUCTION

Gram-negative bacteria ingest sugar through their outer membrane using outer membrane protein (OMP) channels that can be solute specific [1–6]. *Escherichia coli* bacteria utilize glucose-enriched nutrients, so they express the protein channel maltoporin (LamB) to transport maltodextrins, which are glucose-containing oligomers [7–10]. LamB is a trimeric channel, composed of three identical monomers, each of which is barrel shaped with a minimum diameter of a few angstroms [11–16]. A structurally similar trimeric channel called chitoporin (ChiP) is used by species of marine *Vibrio* including *Vibrio harveyi* to transport chitooligosaccharides, allowing the bacteria to utilize chitin biomaterials [17–25].

Studies of *E. coli* and *Salmonella* have revealed that non-coding small RNA control OMP expression, selecting OMP genes in response to growth and stress conditions [26–28]. An unexpressed chitoporin gene was identified in *E. coli*. In the absence of the appropriate inducer, this gene is kept silent by the action of small RNA [29]. However, if *E. coli* is deprived of maltodextrins and exposed to chitooligosaccharides, the chitoporin *Ec*ChiP is expressed, allowing the bacteria to access the available substrate [30].

Recently, we identified and characterized *Ec*ChiP using the black lipid membrane (BLM) reconstitution technique and proved that *Ec*ChiP can readily form a stable pore (see Fig. 1) in artificial phospholipid membranes [31,32]. Microcalorimetry measurements indicate that chitohexaose, a chitosugar, has a strong affinity to *Ec*ChiP. In contrast, no binding affinity for maltohexaose was observed. Here we analyze single-channel current measurements, and the associated sugar trapping and escape dynamics, for the *Ec*ChiP channel.

In the single-channel current measurements [33–36], a potential V is applied across a bilipid membrane perforated with one protein channel in an electrolyte solution with a concentration $[c]$ of sugar on one side of the membrane. The small-ion current $I(t)$ through the open channel is monitored. Since the current decreases to near zero when a sugar molecule is trapped in the channel, $I(t)$ reveals the single-molecule trapping and escape dynamics.

The $I(t)$ data (Fig. 2) for *Ec*ChiP fluctuate between two broad levels, one having a mean value I_0, corresponding to the conductance of the open channel, and the other having a mean I_1 that is essentially zero. In contrast, the current through *Vh*ChiP and *Ec*LamB fluctuates [25,37,38] among four levels $I_n \approx I_0(3-n)$, where I_n is the mean current through a trimer with n monomers blocked by sugar [34,36]. This indicates that *Ec*ChiP is a monomer and thus a convenient system to analyze trapping and escape dynamics free from intermonomer correlations [15,25,38].

The monomer is partly characterized by a trapping rate $k_{\rm on}[c]$ and residence time τ_C, the average time it takes for a trapped sugar molecule to escape the channel. The rate that molecules are transported through the channel Q_T is given by

$$Q_T = k_{\rm on}[c]P_T(1+K)^{-1}, \tag{1}$$

where $K = k_{\rm on}[c]\tau_C$ and it is assumed that no more than one molecule can occupy the channel at a time. The probability P_T that a trapped sugar molecule will be translocated through the channel (as opposed to escaping back to the side of the membrane from which it entered) cannot be obtained directly from the $I(t)$ data. Without some estimate of this parameter, the channel transport efficiency cannot be evaluated.

Below we claim that an estimate of P_T can be obtained from $I(t)$ data. The first step is to extract the probability distribution for the time that molecules remain trapped in the *Ec*ChiP channel, of which τ_C is the mean. This distribution has a

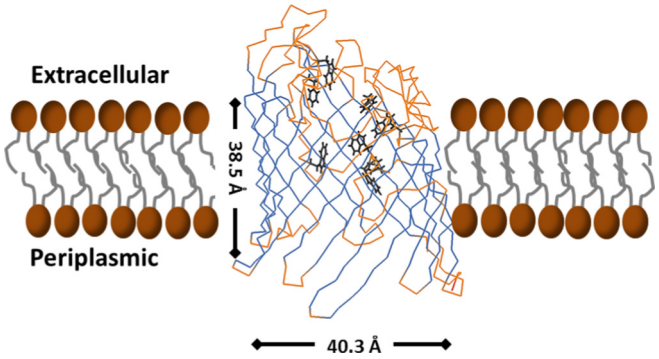

FIG. 1. Illustration of the *Ec*ChiP channel. The ribbon 3D model was generated by SWISS-MODEL [42] using the unpublished structure of *Ec*ChiP complexed with chitohexaose as the structure template. The modeled structure was edited and displayed in PyMOL (for education use only version). The β strands are shown in marine blue (for noncolor plots, the strands in the channel bulk), turns and loops in orange (mainly near the extracellular side in noncolor plots), and the amino acid residues that potentially interact with sugar substrate in the channel are shown as sticks (dark gray hexagonal shapes).

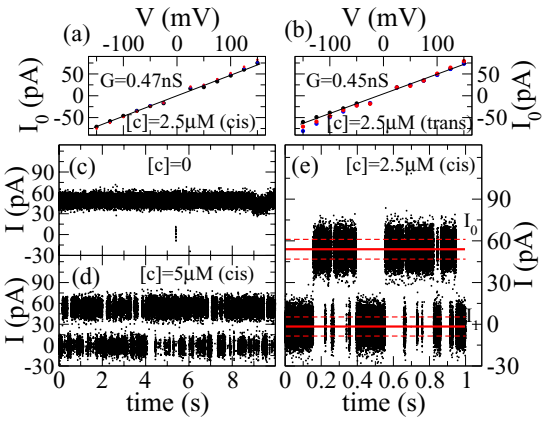

FIG. 2. Current I through a single monomeric channel of *Ec*ChiP with a concentration $[c]$ of chitohexaose in solution, plotted versus applied voltage V and time t. (a) With a concentration $[c] = 2.5$ μM on the *cis* side of the channel, the average current I_0 when the channel is unblocked by sugar versus V satisfies Ohm's law with the conductance G indicated. (b) Same as (a) but with sugar on the *trans* side of the channel. (c) Current $I(t)$ with $[c] = 0$ versus time (the range of time is a small fraction of the total measurement duration). Note that $I(t) \approx I_0$ because the channel is always unblocked. (d) Current $I(t)$ with $[c] = 5$ μM on the *cis* side of the channel. The current changes from $I(t) \approx I_0$ to $I(t) \approx I_1$ when a single sugar molecule blocks the channel. (e) Current $I(t)$ with $[c] = 2.5$ μM on the it cis side of the channel. The horizontal solid lines indicate the current averages I_0 (when the monomer is unblocked) and I_1 (blocked). The dashed lines shown are one standard deviation from these averages.

characteristic time dependence: It exhibits rapid (submillisecond) escape and much slower (10–100 ms) escape. We associate the rapid rate with backward escape processes. Translocation, which requires molecules to negotiate the angstroms wide, nanometers long monomer, proceeds more slowly. The ability to distinguish rapid escape processes, which are dominated by backward escape, from slow escape processes, which likely include a significant contribution from translocation, makes an inference of P_T possible.

We use this analysis to more fully characterize *Ec*ChiP. The escape rate of neutral sugar molecules from *Ec*ChiP is voltage dependent. More precisely, the rapid backward escape rate increases with $|V|$, which lowers transport efficiency. This phenomenon, and other features of trapping and escape processes in *Ec*ChiP, are studied below.

II. MATERIALS AND METHODS

The single-channel current measurements[1] [39–41] employed a cuvette divided into two chambers that are separated by a 25-μm-thick Teflon barrier with a circular aperture 60–100 μm in diameter. An electrolyte solution, 2.5 ml of 1 M KCl in 20 mM HEPES pH 7.5, is introduced to both chambers and Ag/AgCl electrodes are positioned on respective sides of the barrier. When 2–5 μL of 5 mg mL^{-1} 1,2-diphytanoyl-*sn*-glycero-3-phosphatidylcholine (Avanti Polar Lipids, Alabaster, AL) in n-pentane is added to both chambers, a lipid bilayer forms over the aperture after the lipid concentration in the electrolyte is gently raised and lowered several times by pipetting. To perforate the lipid bilayer with a single channel, 50–100 ng/mL of *Ec*ChiP is added to one *cis* side of the membrane with a potential ± 100 mV across the artificial membrane, until a step increase of the ionic current $I(t)$ is observed. The protein solution is then diluted by sequential additions of electrolyte to prevent further channel insertions.

The potential of the electrode in the *cis* chamber, to which *Ec*ChiP is added, is defined to be zero. A potential V that can be positive or negative is applied to the electrode on the *trans* side. Sugar is added to one side of the membrane, so in some cases the sugar diffusion current flows in the same direction as the electric current and in others it flows against it.

From the raw $I(t)$ data (Fig. 2), it is possible to distinguish states with $I(t) \approx I_0$, when the *Ec*ChiP monomer is open, from states with $I(t) \approx I_1$, when the monomer is blocked. In the absence of sugar, the current $I(t)$ fluctuates about an average value I_0. With $V = 100$ mV, we see a mean $I_0 \approx 45$ pA (corresponding to a conductance $G = 0.45$ nS) and standard deviation σ_0 of about 8 pA. When sugar is added, larger fluctuations in $I(t)$ are observed: The current drops to a value near zero [after the current decrease, $I(t)$ fluctuates about an average value I_1 of a few picoamperes with a standard deviation similar to σ_0].

Using the pCLAMP10 software, we record stable events in which $I(t)$ remains near I_j for a time greater than $t_{\min} = 0.1$ ms. If one zooms in on $I(t)$ data to see the transition between I_j levels, the duration of a transition is smaller than $t_{\min}$ by a factor of order unity (when a molecule blocks the channel current, it creates an effective capacitor that requires finite time to charge or discharge). Since $I(t)$ requires time of order $t_{\min}$ to respond to a trapping or escape event, shorter events are unobservable in the experiment.

[1] All current measurements were performed with an Axopatch 200B amplifier (Molecular Devices, Sunnyvale, CA, USA) in the voltage clamp mode, with the internal filter set at 10 kHz.

Regarding the chitosugars used for the current measurements, chitooligosaccharides, including chitopentaose, chitohexaose, and chitosan hexaose, were purchased from Dextra Laboratories (Science and Technology Centre, Earley Gate, Reading, United Kingdom) and Megazyme (IDA Business Park, Bray, Co., Wicklow, Ireland).

To obtain the structural prediction illustrated in Fig. 1, the amino acid sequence of the EcChiP (UniProtKB entry P75733) was submitted to SWISS-MODEL [42] for tertiary structure prediction using the three-dimensional (3D) structure of Pseudomonas aeruginosa OprD (pdb 2odj) as structural template [43]. The annotated structures were edited and displayed in PyMOL [44].

III. RESULTS AND DISCUSSION

A. Single-channel current data and its analysis

The current $I(t)$ passes through a single *Ec*ChiP channel embedded in the bilipid membrane. An illustration of the channel appears in Fig. 1. The length of the channel is several nanometers and the diameter of its mouth is similar. The internal structure of the channel, formed from a polypeptide chain with both the N and C terminals on the periplasmic side, is complex. Within the channel interior, the effective diameter is as small as a few angstroms. There are numerous amino acid residues, also shown in Fig. 1, arranged on the outer wall of the channel barrel with others part of extracellular loops. Fluorescence results indicate an interaction between sugar molecules and the tryptophan members, in particular, of the amino acid residues [32].

The structure has significant *cis-trans* asymmetry. In previous studies with *E. coli* LamB [40,43,45,46], it was observed more than 70% of the reconstituted channels are oriented with the extracellular side facing the chamber to which the channel precursor was added. If this tendency holds for the *Ec*ChiP channels studied here, then the *cis* end of the channel in typical current measurements should correspond to the extracellular side *in vivo*. This is further suggested by the *Ec*ChiP channel structure itself, with long hydrophilic extracellular loops that are likely not amenable to channel insertion. However, we will not assume that the *cis* side of the membrane corresponds to the extracellular solution below, and will compare $I(t)$ data with sugar introduced to each chamber.

In Fig. 2, a one-second segment of a current trace is shown. Transitions between the I_0 and I_1 states are clear. The time-averaged current passing through an open channel I_0 is plotted versus the applied voltage in the presence of chitohexaose on the *cis* or *trans* sides of the membrane. The current satisfies Ohm's law with $I_0 = GV$ and $G \approx 0.45$ nS with a fitting error of 2% over the range indicated (the error in the time-averaged current and the applied potential are too small to appear on this scale; one expects t- and V-dependent changes in the complex monomer to introduce greater uncertainty). If we write the conductance as $G = (\pi a^2/d)\rho^{-1}$ with a and $d = 4$ nm the effective radius and length of the channel, respectively, and ρ the resistivity of the KCl solution, then we find an effective channel diameter of $2a \approx 0.5$ nm. (This diameter, considerably smaller than that of the channel mouth seen in Fig. 1, corresponds to the narrow channel interior.) In comparison, an open channel of trimeric *Vh*ChiP has a larger conductance of 1.6–1.8 nS.

The statistical description of the I_j events can be displayed using a cumulative histogram that counts the number of events with a duration greater than a given t. We define $f_j(t)$ as the fraction of I_j events having a duration greater than t (the height of the cumulative histogram divided by the total number of I_j events). For an infinite number of events, $f_j(t)$ would be a continuous function giving the probability for an I_j event that began at $t = 0$ to survive beyond t. The smooth curves of $f_j(t)$ data approximate this probability. The average trapping rate $k_{\rm on}[c]$ and residence time τ_C are simply related to $f_0(t)$ and $f_1(t)$,

$$1/k_{\rm on}[c] = \int_0^\infty dt\ f_0(t), \quad \tau_C = \int_0^\infty dt\ f_1(t). \tag{2}$$

Since $f_j(t)$ decreases by orders of magnitude over the time range of interest, it is convenient to introduce logarithms. These logarithms have a simple physical interpretation. The slope $d/dt[-\ln f_0(t)]$ is the instantaneous trapping rate, i.e., the probability rate for a monomer that has been continuously open for time t to become blocked. If this trapping rate is a constant then $\ln f_0(t)$ is linear in time: $\ln f_0(t) = -k_{\rm on}[c]t$ and thus $f_0(t)$ is a simple exponential $f_0(t) = \exp(-k_{\rm on}[c]t)$. Similarly, $d/dt[-\ln f_1(t)]$ is the escape rate, the probability rate for a monomer that has been continuously blocked for time t to become unblocked. If the escape rate is constant and equal to $k_{\rm off}$ then $\ln f_1(t) = -k_{\rm off}t$ with $k_{\rm off} = 1/\tau_C$ and $f_1(t) = \exp(-k_{\rm off}t)$.

In all data considered, the initial number of events $N_j(t_{\rm min})$ varied between several hundred (at low $[c]$) to more than 5000 and decreased according to $N_0(t) = N_0(t_{\rm min})f_0(t)$ and $N_1(t) = N_1(t_{\rm min})f_1(t)$. At small t, the sampling error, proportional to $\sqrt{N_j(t)}$, is of order 1% of the measured $N_j(t)$. At large times, the sample size has decreased to a point that the sampling error is a significant fraction of $N_j(t)$. This is reflected by the noisy appearance of $f_1(t)$ at large t. One sees significant variation between $f_1(t)$ curves measured for different *Ec*Chip channels. With regard to prediction of transport properties, this channel-to-channel variance is the greatest source of uncertainty. The probabilities $f_0(t)$ and $f_1(t)$ are defined over a range $t_{\rm min} < t < t_{\rm max}$, where $t_{\rm min} = 0.1$ ms is the threshold for observable events, with $f_0(t_{\rm min}) = f_1(t_{\rm min}) = 1$ and $t_{\rm max}$ defined such that at least ten I_j events survive until $t_{\rm max}$.

B. Trapping and detrapping of sugar by chitoporin

Figure 3 presents experimental results for $f_0(t)$ and $f_1(t)$ obtained with varying chitohexaose concentration $[c]$ introduced to the *cis* and *trans* chambers. For these data, the applied voltage was fixed at $V = -100$ mV, so the electric current flows from the *cis* to the *trans* chamber. As seen in Fig. 3, the histograms of $f_0(t)$ and $f_1(t)$ are difficult to interpret visually, but their logarithms yield smooth curves that are more convenient to analyze.

The plots of $\ln f_0(t)$ show a linear t dependence, with a slope that increases with sugar concentration $[c]$. The trapping probability $f_0(t)$ is strongly dependent on concentration $[c]$, so $-\ln f_0(t) \approx k_{\rm on}[c]t$, where the slope $k_{\rm on}[c]$ increases monotonically with sugar concentration $[c]$.

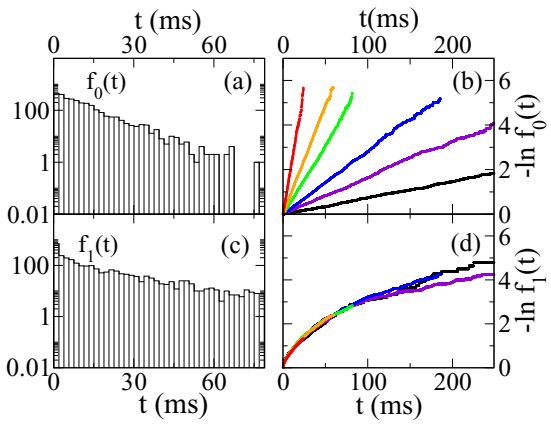

FIG. 3. Channel trapping and escape probabilities versus time t with a concentration $[c]$ of sugar on the *cis* side of the channel. (a) Histogram, for $[c] = 20\ \mu$M, of the probability $f_0(t)$ for the channel to remain unblocked beyond time t given that it became unblocked at $t = 0$. (b) Logarithm of $f_0(t)$. The curves (black, violet, blue, green, orange, and red, from the bottom to the top) show $[c] = 1.25$, 5, 10, 20, 40, and 80 μM, respectively. They are linear with a slopes indicating the rate at which sugar molecules are trapped. (c) Histogram, with $[c] = 20\ \mu$M, of the probability $f_1(t)$ for the channel to remain blocked beyond time t after becoming blocked at $t = 0$. (d) Logarithms of $f_1(t)$ for different values of $[c]$ (same values and colors as in (b); for noncolor plots, the result is approximately $[c]$ independent). The nonlinear curves indicate that sugar molecules can escape the channel at multiple rates.

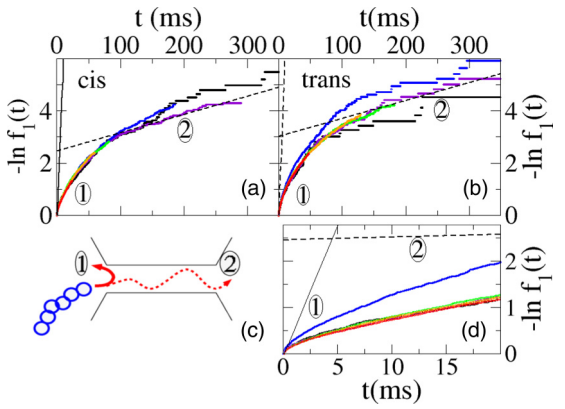

FIG. 4. Inferring the probability of sugar translocation from the nonlinear time dependence of $\ln f_1(t)$. (a) Logarithm of $f_1(t)$ for sugar concentration $[c] = 1.25$, 5, 10, 20, 40, and 80 μM on the *cis* side of the chamber (black, violet, blue, green, orange, and red curves; for noncolor plots, the $[c]$ dependence is weak). The two thin lines show linear fits made at small t and large t. (b) Same as (a) but with sugar on the *trans* side. The $\ln f_1(T)$ curves exhibit a rapid t dependence at small t, the region labeled 1, and a slow linear dependence at large t, labeled 2. (c) A plausible picture, illustrated by the cartoon, is that 1 is associated with chitohexaose molecules escaping back to the side of the channel from which they entered, while translocation through the channel occurs during 2. (d) Same data as in (b) plotted on a timescale within region 1. The linear fit from region 2 is shown as the dashed line.

On the other hand, $\ln f_1(t)$ is approximately $[c]$ independent and nonlinear in time. As seen in Fig. 4, its behavior is similar whether sugar approaches from the *cis* or *trans* chambers. The escape rate, given by the slope of $\ln f_1(t)$, is largest at the minimum time of $t = t_{\min}$, decreases with t, and appears to approach a constant at large t. Linear fits to the curves yield slopes that are two orders of magnitude larger at $t_{\min}$ than at large t. That is, molecules that have recently become trapped in the channel escape at a much higher rate than those that have already been bound for an extended period.

In Fig. 4, the evolution of $\ln f_1(t)$ is described in terms of two distinct regions. At low t, in the so-called region 1, the $\ln f_1(t)$ curve is nonlinear and changes rapidly with time. At large t, region 2, the curve is linear with a much smaller slope and can be approximated by

$$-\ln f_1(t) \approx B_0 + \lambda_1 t \quad (\text{large } t), \tag{3}$$

where λ_1 is the slope at large t and B_0 is the extrapolated $t = 0$ intercept. Data below indicate that behavior in the two regions responds differently to control parameters like applied voltage and the the size of the sugar molecule.

A plausible picture, illustrated by the cartoon in Fig. 4(c), is that the behavior of $f_1(t)$ in region 1 is dominated by events in which a molecule that has just been trapped escapes back to the side of the channel from which it entered. The small-t dependence of $f_1(t)$ is attributable to backward escape of molecules. Slower events, in which the molecule traverses the length of the channel and is translocated to the other side of the membrane, contribute to $f_1(t)$ in region 2. That is, during the large-t region in which $\ln f_1(t)$ is linear, translocation events are likely. If this picture turns out to be valid, then the time dependence of $f_1(t)$ can be used to estimate the translocation probability P_T.

Suppose we make the bold assumption that all translocation occurs during the large-t regime (region 2) and all backward escape occurs earlier (during region 1). Then the fraction P_T of I_1 events that end with translocation is equal to the fraction of events that end during the large-t regime. That is, $P_T \approx \exp(-B_0 - \lambda_1 t^*)$, where t^* is the time when the large-t region begins. Since $B_0 > \lambda_1 t^*$ in Fig. 4, we can approximate this by $P_T \approx \exp(-B_0)$. So

$$\tilde{P}_T \equiv \exp(-B_0) \tag{4}$$

would provide an experimental measurement of the translocation probability P_T. For the data of Fig. 4 it gives $\tilde{P}_T = 0.1$ and 0.05 for sugar approaching from the *cis* and *trans* sides. The uncertainty in these estimates may be as high 50% (though much less in favorable examples). The standard error of linear fits is small (usually less than 1%), but a greater uncertainty may be associated with choosing the high-t range over which to fit. If one sees significant variation of $\tilde{P}$ with concentration $[c]$ (and assumes that such a $[c]$ dependence is not a real effect) then the difference between $\tilde{P}_T$ values obtained from different $[c]$ curves may be considered a measure of uncertainty as well.

In the Appendix, we consider a simplified model of monomers and calculate $f_1(t)$ and P_T. We model the monomer as a sequence of many trapping sites, through which a sugar molecule performs a random walk. The resulting $f_1(t)$ is qualitatively similar to the data of Fig. 3. According to the model results, the initial slope of $\ln f_1(t)$ corresponds to events where a molecule escapes backward immediately after

being trapped. At small t (prior to the large-t linear regime), molecules can wander a few steps into the channel before escaping backward. Translocation events occur at longer t and contribute a significant fraction to the large-t linear regime of $f_1(t)$. The quantity $\tilde{P}_T$ agrees roughly with P_T (overestimating it by a factor of order unity that depends on the details of the random-walk parameters).

We are claiming that $\tilde{P}_T$ is a reasonable proxy for the translocation probability P_T. If a distinct t-linear region of $\ln f_1(t)$ is observed at large t then $\tilde{P}_T$ can be measured.[2] In the following sections, we provide some experimental support for this claim.

C. Voltage-dependent trapping of charged chitosan

Chitosan hexaose is structurally similar to chitohexaose. At neutral pH, the molecule lacks the N-acetyl group at C2 of the glucosyl ring and is electrically neutral. However, in acidic solutions, it acquires a positive charge via the primary amine at the C2 position. We have measured the single-channel current through *Ec*ChiP in an acidic solution, pH of 5.5, with a concentration $[c]$ of chitosan hexaose (instead of the usual chitohexaose).

The trapping of chitosan hexaose is strongly voltage dependent because the charged molecule experiences the electric field associated with V. We can exploit this dependence to show that the small-t behavior of $f_1(t)$ is dominated by backward escape.

When chitosan hexaose is introduced to the *cis* chamber with $V < 0$ or the *trans* chamber with $V > 0$, the molecular diffusion current flows in the same direction as the electric current. Molecules are pushed towards the channel by the electric field, so $k_{on}[c]$ should increase with $|V|$. Once a molecule is trapped, the field pushes it deeper into the channel, so the probability of translocation P_T should increase with increasing $|V|$. With the sign of V reversed, the trapping rate should be small and backward escape dominant over translocation.

In Fig. 5, we show plots of the logarithms of $f_0(t)$ and $f_1(t)$ measured for $[c] = 5$ μM of chitosan hexaose introduced to the *cis* side and *trans* sides of the channel for different values of V. The main panels describe molecules flowing with the electric current.

The function $\ln f_0(t)$ is linear in t with a slope $k_{on}[c]$. When chitosan hexaose flows with the electric current, $k_{on}[c]$ increases with $|V|$. When it flows against the current [shown in the insets of Figs. 5(a) and 5(b)], the logarithm of $f_0(t)$ is noisy and does not exhibit a systematic $|V|$ dependence.

In Figs. 5(c) and 5(d), the logarithm of $f_1(t)$ exhibits its usual nonlinear t dependence. There is an evident V dependence, with $f_1(t)$ changing less rapidly at small t when

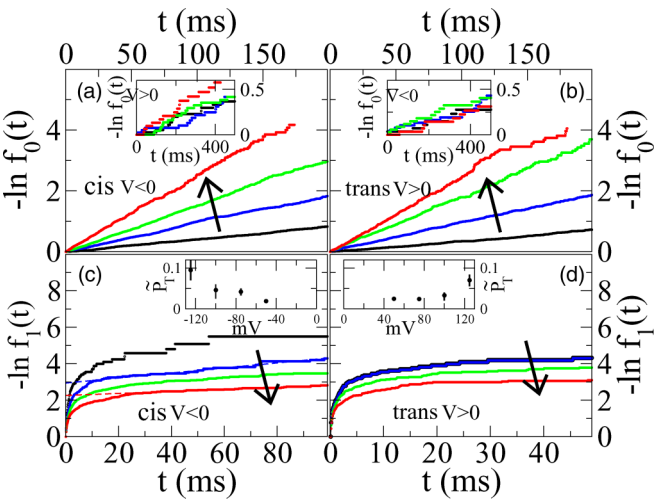

FIG. 5. Trapping and escape with a concentration $[c] = 5$ μM of chitosan hexaose molecules in acidic solution, in which the molecule acquires a positive charge, with the electrode on the *trans* side at a voltage V relative to the *cis* side. (a) Plots of $\ln f_0(t)$ for molecules on the *cis* side of the membrane, driven towards the channel by the voltage $|V| = 50$, 75, 100, and 125 mV (respectively, along the arrow). The trapping rate, given by the slope of $\ln f_0(t)$, increases with driving voltage. The inset shows that the polarity of the potential is reversed, so molecules are pushed away from the channel. (b) Same as in (a) but with the chitosan on the *trans* side of the channel. (c) Plots of $\ln f_1(t)$ for the same conditions as in (a). The escape rate, given by the slope of $\ln f_1(t)$, decreases with driving voltage at small t but is approximately V independent at large t. The inset shows that the parameter $\tilde{P}_T$, which we propose as the approximate probability for molecules to be translocated through the channel, increases with driving voltage. (d) Same as in (c) but with the chitosan on the *trans* side of the channel.

$|V|$ is increased. That is, when the applied voltage V pushes the chitosan hexaose molecules into the channel, the probability of rapid escape decreases with the driving force $|V|$. This trend is understandable if $f_1(t)$ is dominated by backward escape for $t < 1$ ms. As $|V|$ is increased, the rate of backward escape is reduced, which explains why the escape rate at low t decreases.

Fits of $-\ln f_1(t) \approx B_0 + \lambda_1 t$ at large t yield λ_1 values that are weakly $|V|$ dependent and an intercept B_0 that decreases with increasing $|V|$. The plot of $\tilde{P}_T$ versus V in Fig. 5 shows that this quantity increases rapidly with voltage when sugar molecules flow with the electric current, as expected. (The error bars were obtained by selecting various possible high-t ranges over which to perform linear fits.) In equilibrium, a trapped molecule with charge q is more likely to escape to the low-V side by a factor $\exp(qV/kT)$. This factor is large (between 7 and 400) over the range of V shown, so the relatively small $\tilde{P}_T$ may indicate a large kinetic barrier that acts against translocation. The data here are not sufficient to analyze this feature quantitatively.

The qualitative results of Fig. 5 indicate that the physics of the rapid escape processes that determine $f_1(t)$ at small t is different from that of processes that determine $f_1(t)$ at large t. The large-t, V-independent detrapping processes must be associated with either translocation or backward escape occurring at a rate slower by two orders of magnitude than

[2] In some $f_1(t)$ data, the high-t linear regime is limited to a relatively small number of events or perhaps not evident at all. Intercepts extrapolated from high t will then tend to give $\tilde{P}$ that are too large. These cases correspond to small P_T, where low-t (back-escape) processes dominate the data. So $\tilde{P}_T$ provides an estimate of P_T when translocation is likely and a useful upper limit when translocation is rare.

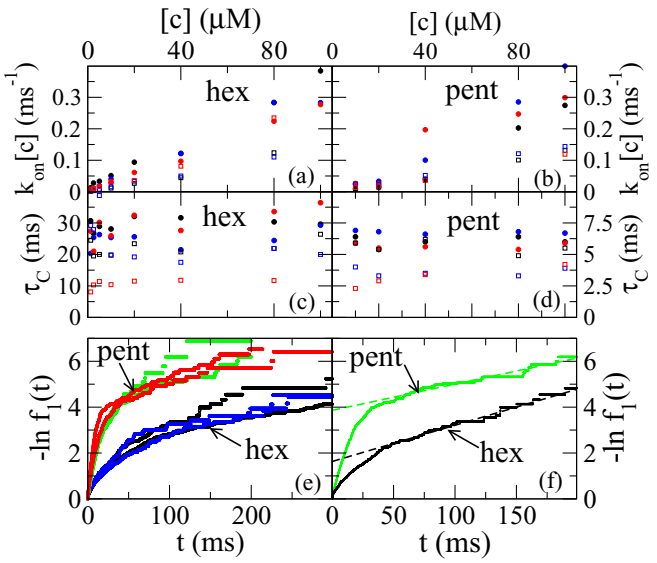

FIG. 6. Trapping and escape rates of different chitosugar molecules with concentration $[c]$ and an applied voltage $|V| = 100$ mV. (a) Trapping rate $k_{on}[c]$ of chitohexaose on the *cis* side (closed circles) and *trans* side (open squares) of the channel. Different curves are different channel samples measured under the same conditions. (b) Same as (a) but for chitopentaose. (c) Average residence time of chitohexaose τ_C, for the same experiments as in (a). (d) Same as in (c) but with chitopentaose. (e) Logarithm of $f_1(t)$, measured for two channel samples with sugar added to the *cis* (black and green) and *trans* (blue and red) sides at concentration $[c] = 1.25$ μM for chitohexaose and $[c] = 10$ μM for chitopentaose (for noncolor plots, differences between colored curves are insignificant). (f) Two curves from (e), with linear fits made at high t shown as dashed lines.

occurs at small t. When chitosan hexaose flows opposite to the electric current, $f_1(t)$ can only be measured (data not shown) at extremely small t. There were no observed I_1 events with a duration of more than a few milliseconds, so the long-t behavior of $f_1(t)$ is absent.

The data of Fig. 5 indicate that the rapid initial variation of $f_1(t)$ is due mainly to backward escape of chitosan hexaose molecules. The measured $f_1(t)$ curves are qualitatively similar for chitosan hexaose and chitohexaose, so it is reasonable to attribute the small-t behavior of $f_1(t)$ with backward escape for chitohexaose as well. We have no direct evidence for translocation of chitohexaose from the current measurements but, given the biological function of the channel, it presumably occurs [30]. This translocation can only happen for larger values of t, after the initial rapid variation of $f_1(t)$ has ended. In light of chitosan data, the claim that $\tilde{P}_T \gtrapprox P_T$ seems more likely.

D. Comparing the translocation probability of different chitosugars

We study the dependence of $k_{on}[c]$, τ_C, and $\tilde{P}_T$ on experimental variables. In particular, we can compare the single-molecule dynamics for different-sized chitosugars: chitohexaose and chitopentaose. In Fig. 6, the trapping rate $k_{on}[c]$ and residence time τ_C are shown for several different channel samples, with sugar at a concentration $[c]$ introduced to the *cis* and *trans* sides.

When trapping is measured for different channel samples, significant differences are seen. This variation between samples is the largest source of error in characterizing transport properties (the statistical fitting error in k_{on} and τ_C, which are obtained from data sets with several thousand points, are negligible in comparison and would not even be visible on this scale).

For chitohexaose introduced to the *cis* side of the membrane, the three channels have trapping rates that differ by about 30% at high $[c]$. Larger differences are seen with sugar approaching from the *trans* side of the membrane. The magnitude of $k_{on}[c]$ for chitohexaose and chitopentaose appear similar in these data. The residence time τ_C is independent of $[c]$, varies significantly from sample to sample, and is roughly five times larger for chitohexaose than for chitopentaose.

The logarithm of $f_1(t)$ is shown for both chitohexaose and chitopentaose on the *cis* and *trans* sides of the membrane. The quantitative details depend on the sample and on whether sugar approaches from the *cis* or *trans* side but the qualitative t dependence is robust. A difference between $f_1(t)$ measured for chitohexaose and chitopentaose is evident: The latter changes more rapidly at small t. The chitopentaose data shown were obtained at higher $[c]$, because the rapid drop of $f_1(t)$ depletes the sample size of events and limits the measurable range at low $[c]$. Since $f_1(t)$ is $[c]$ independent, we choose $[c]$ values that give a larger range and less noisy data.

In Fig. 6(f), representative plots of ln $f_1(t)$ for chitohexaose and chitopentaose are compared and high-t linear fits shown. The large-t slope, indicating the escape rate of the longest-residing sugar molecules, is similar for the two sugars. However, the rapid initial change of f_1 for chitopentaose results in a larger B_0 value. The associated value of $\tilde{P}_T$ is roughly 0.2 for chitohexaose and 0.02 for chitopentaose.

When chitopentaose is trapped within the *Ec*ChiP channel, it has a high probability to escape within a millisecond. Trapped chitohexaose molecules are less likely to escape so rapidly and have a relatively high probability to be retained within the channel for a duration of 10 ms or greater. The larger chitohexaose molecules thus enjoy a greater opportunity to be translocated and would, according to Eq. (1) under the assumption $P_T \approx \tilde{P}_T$, be transported through the membrane ten times more rapidly at low $[c]$.

E. Voltage-dependent trapping dynamics for neutral chitohexaose

In Fig. 7, the trapping and detrapping characteristics for chitohexaose are shown as a function of applied voltage. The charged chitosan hexaose molecules were understandably affected by the applied potential. For neutral chitohexaose, the V dependence is more difficult to predict. It turns out that there is a significant V dependence, especially in $f_1(t)$, but it is qualitatively different from that seen for chitosan hexaose. The trapping and escape dynamics for neutral chitohexaose are sensitive to the magnitude $|V|$ of the potential, but independent of its sign.

In Fig. 7, the trapping rate $k_{on}[c]$ at a fixed $[c] = 5$ μM is plotted versus applied voltage. With sugar on the *cis* side of the

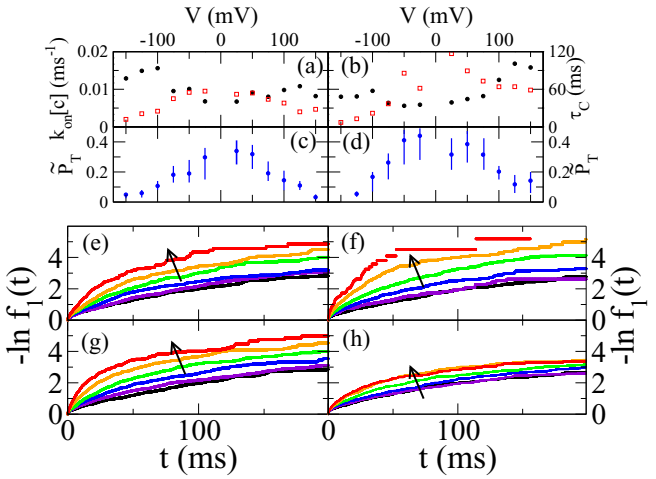

FIG. 7. Trapping and escape of neutral chitohexaose molecules as a function of the voltage V of the electrode on the *trans* side (with the *cis* electrode at ground). (a) Average trapping rate $k_{on}[c]$ (closed circles) and residence time τ_C (open squares) with sugar concentration $[c] = 5\ \mu$M on the *cis* side of the channel. (b) Same as in (a) but with sugar on the *trans* side. (c) Parameter $\tilde{P}$, proposed as the probability for sugar molecules to be translocated through the channel, for the same conditions as in (a). (d) Same as in (c) but with sugar on the *trans* side. (e) Logarithm of $f_1(t)$, with $[c] = 5\ \mu$M on the *cis* side and $V > 0$. Different curves are for $|V| = 25$, 50, 75, 100, 125, and 150 mV along arrow (black, violet, blue, green, orange, and red curves, respectively). (f) Same as in (e) but with sugar on the *trans* side and $V < 0$. (g) Same as in (e) but with $V < 0$. (g) Same as in (f) but with $V > 0$.

membrane, the sugar flows in the same direction as the electric current when $V < 0$ and in the opposite direction when $V > 0$. Starting from large negative values of V and increasing, the trapping rate first decreases, with an interpolated minimum at $V = 0$, and then slightly recovers at large positive V. The changes in $k_{on}[c]$ with V are of the order 50% of its maximum value. The data for sugar on the *trans* side exhibit a V dependence that mirrors the result with sugar on the *cis* side. The fitting error in the $k_{on}[c]$ and τ_C values shown is of order 1% but, as discussed in the preceding section, the much larger variation between channels gives a better indication of their uncertainty.

The effect of varying V on the probability $f_1(t)$ for chitohexaose is shown in Figs. 7(e)–7(h). For sugar on either side of the channel and either sign of V, the function $f_1(t)$ increases more rapidly at small t as the strength of the driving potential is increased. [The magnitude of $\ln f_1(t)$ at $t = 1$ ms increases by a factor of 2 when V increases from 25 to 150 mV.] That is, an applied voltage apparently increases the rate of backward escape by recently trapped chitohexaose molecules. The probability of translocation, as indicated by $\tilde{P}_T$, decreases with $|V|$. The large-t escape rate λ_1 is approximately independent of $|V|$.

The dependence of $f_1(t)$ on $|V|$ is suggestive of an induced polarization effect. Suppose that the large (and assumed constant) electric field in the channel $|E| \approx |V|/d$, where the channel length $d \approx 4$ nm, results in an average polarization density $\mathbf{P} = \chi\epsilon_0\mathbf{E}$. If the polarization of a monomer in an open state is different from that of a monomer obstructed by a sugar molecule then, when the sugar molecule escapes, there is a change in electrostatic energy $\Delta E = -\epsilon_0\chi(V/d)^2\Delta\Omega$, where $\Delta\Omega$ is a parameter with the dimension of volume that is used to account for the polarization change. (A change in the susceptibility χ can be absorbed into $\Delta\Omega$ and thus χ taken to be the same for both states.)

The energy difference appears in a Boltzmann factor modifying the reaction rate for a molecule to transition from a bound state inside the channel to an itinerant state in the ambient solution. In a model with multiple bound states for a sugar molecule (like that considered in the Appendix), the measurable escape rate of sugar molecules depends not only on this final reaction rate, but also on the rate of transitions between the internal bound states (which would presumably be weakly affected by the polarization energy and potential V). However, if the Boltzmann factor is rate limiting for the rapid escape observed at the time $t = t_{min}$, then $\Lambda = \Lambda(V) \equiv -(1/f[t_{min}])\ln f_1[t_{min}]$ should be proportional to this Boltzmann factor

$$\Lambda(V) \approx \Lambda(0)\exp\left(C\frac{[eV]^2}{[k_BT]^2}\right), \tag{5}$$

where

$$C = \Delta\Omega\frac{\chi\epsilon_0 k_B T}{e^2 d^2}. \tag{6}$$

For positive $\Delta\Omega$ values, Eq. (5) predicts that the escape rate $\Lambda(V)$ will increase with $|V|$.

In the data shown above, the factor $(eV)^2/(k_BT)^2$ varies from roughly 1 to 36. For an order-of-magnitude upper estimate of C, we describe the channel as a number volume n of independent molecular dipoles in thermal equilibrium that are aligned by the field and write $\chi\epsilon_0 \approx ne^2a^2/k_BT$, where a is a length scale for the dipole, giving $C = (n\Delta\Omega)(a/d)^2$. Taking a to be an atomic distance, $n \approx 1/a^3$, and $\Delta\Omega$ to be the volume of the channel interior, we get $C \approx 1/20$. This value would result in Λ changing by a factor of more than 6 when V increases over the measured range. While this is clearly a crude treatment, it does provide a possible approach to understanding the qualitative V dependence of the detrapping characteristics. It may be noted that, in Ref. [41], the authors suggested that a V-dependent τ_C observed in LamB may arise because an applied voltage may cause, in addition to a dipole energy effect, a transition of an open monomer to a different configuration with a reduced sugar-binding affinity (i.e., a gating transition). However, if the small ion conductance of the two configurations is different, then Ohm's law would be violated, which does not appear to be compatible with Fig. 1.

As seen earlier for charged chitosan hexaose, the small-t behavior of $f_1(t)$ changes with V but the large-t escape rate λ_1 is V independent. Upon initially being trapped, the molecule has a backward escape rate that increases with $|V|$. Once a molecule moves into the channel, it is no longer susceptible to backward escape. If it maneuvers to a position from which it can escape to the opposite chamber, then this final escape rate would be enhanced by $|V|$ according to the energetic argument above. However, the long-term escape rate will be independent of V provided the propagation through the channel is rate

limiting (the model calculations in the Appendix are relevant to this discussion).

IV. DISCUSSION

In the results above and those of our earlier studies of *Vh*ChiP, the probability for the channel to remain unoccupied $f_0(t)$ decays as a single exponential with a $[c]$-dependent rate. The statistics of trapping can thus be characterized by a single value, the rate $k_{\rm on}[c]$. This quantity is linear in $[c]$, as seen in Fig. 6, giving a value of $k_{\rm on}$ that is $[c]$ independent. Its value varies considerably from channel sample to sample and depends on the applied voltage, but it is roughly the same whether sugar approaches from the *cis* or *trans* side of the membrane and is of order 2×10^5 M^{-1} s^{-1} for $V = 100$ mV. This value of $k_{\rm on}[c]$ is close, at a given value of $[c]$, to the trapping per monomer observed in *Vh*ChiP.

The probability for the channel to remain occupied by sugar $f_1(t)$ does not decay as a single exponential. The escape statistics cannot be described by a single parameter, such as the average residence time τ_C or its inverse $k_{\rm off} = 1/\tau_C$. The effective escape rate changes depending on how long the sugar molecule has remained bound in the channel. Molecules bound for the minimum measurable duration of $t_{\rm min}$ have an escape rate of order 1 ms^{-1}, while those that remain in the channel for at least tens of milliseconds escape at a slower rate of $\lambda_1 \approx 10$ s^{-1}.

The average time that a chitohexaose molecule remains bound τ_C, which varies considerably from sample to sample and depends on the applied voltage is, for $|V| = 100$ mV, of order 20 ms (it does not depend much on whether sugar was introduced to the *cis* or *trans* side of the channel). Combining these average results, one obtains a equilibrium constant $k_{\rm on}\tau_C$ of order 10^5 M^{-1}. These values are consistent with values obtained from current averages for other samples and reported in Ref. [32].

The time dependence of the effective escape rate lends itself to physical modeling of the monomer. The simplest model has a single trapping configuration for a sugar molecule. A molecule approaching from either side of the membrane can be trapped in this configuration and may later escape to either side. Assuming constant trapping and escape probability rates, $f_1(t)$ is a simple exponential function, inconsistent with the experimental data. We are thus led to consider models with multiple trapping configurations. We suppose that a molecule that approaches from the *cis* end of the channel and becomes trapped within the monomer can immediately escape back to the *cis* side. If the molecule is to escape to the *trans* side, it must first progress via intermediate transition states, delaying translocation.

A simple example of this latter type of model is the 1D random walk of the Appendix, in which a series of binding sites is located along the channel length. It produces $f_1(t)$ behavior in qualitative agreement with the data. The probability $\ln f_1(t)$ changes rapidly at small t because of the high rate for recently trapped molecules to escape back into the chamber from which they just arrived. If the molecule remains bound for an extended time then it typically moves deep into the channel. From here, escape becomes more difficult and the associated rate decreases, but the molecule can eventually escape to either side of the channel. The probability $f_1(t)$ is a single exponential with an escape rate λ_1 at large t. If such a model is applicable, then it is possible to estimate the probability of sugar translocation from the $f_1(t)$ data.

Our recent attempt [32] to characterize the *Ec*ChiP channel suggests the complex structure of Fig. 1. There are numerous amino acid residues arranged along the length of the channel interior. Fluorescence results indicate an interaction between sugar molecules and the Trp residues, in particular, offering some insight into the sugar binding and transport mechanism. It is plausible that the locations of the residues are important trapping sites and may be associated with an observable sugar binding energy.

Microcalorimetry measurements revealed a binding energy of order a significant fraction of 1 eV for a single chitohexaose molecule. The Boltzmann factor associated with escaping such a bound state is of order 10^{-9}. If we assumed a preexponential frequency typical of molecular vibrations, then this would suggest an escape rate of order 0.1 ms^{-1} or smaller. However, any attempt to make a quantitative comparison between the thermodynamic binding energy and a measured escape rate like the large-t rate λ_1 is complicated by several factors. For example, we do not know the maximum escape rate because only molecules bound for more than $t_{\rm min}$ can be observed via the current measurement (thus, a basic escape rate like Λ_0^- used in the model of the Appendix is not observed via the current measurement). Also, in a model with multiple binding configurations with different energies, we would have to obtain an effective binding energy as an appropriate weighted average. Nevertheless, establishing a connection between the phenomenological model of sugar transport discussed in this paper and a more realistic description of the monomer structure is of interest (see, for example, Ref. [47]).

The complex three-dimensional structure of the monomer bears little resemblance to the one-dimensional chain described in the Appendix. Moreover, the model structure of Fig. 1 exhibits a pronounced *cis-trans* anisotropy, which was not evidenced by the trapping and escape statistics: $f_0(t)$ and $f_1(t)$ were qualitatively similar for sugar approaching from either end of the channel. However, making a correspondence between the realistic structure and model calculations, one must consider the following. Different binding configurations could describe not only the physical position of the sugar molecule, but also conformational changes of the molecule within the monomer. The position of the binding site along the chain can be interpreted as a more general reaction coordinate that spans the range of accessible bound configurations. As a minimal assumption, we could suppose that all such bound states can be roughly grouped into three categories: states accessible to a molecule entering (i) from the *cis* chamber, (ii) from neither chamber, and (iii) from the *trans* chamber. This is sufficient to obtain a $f_1(t)$ function with the same qualitative time dependence as the experimental result with translocation mainly occurring on long-t scales. Thus, just as in the simplistic chain model detailed in the Appendix, translocation probability can be approximated from $f_1(t)$. The one-dimensional picture may be regarded as an illustrative example of the class of models needed to understand the $I(t)$ data and its relation to sugar transport.

The $I(t)$ data do not reveal to which side of the channel a trapped molecule escapes. Our argument that the translocation probability P_T can nonetheless be inferred from $I(t)$ data is based on the following points. First, $f_1(t)$ has a qualitative t dependence that is compatible with models that predict backward escape at small t and translocation at large t. Second, $f_1(t)$ for charged chitosan hexaose has the same t dependence as chitohexaose but for chitosan hexaose the initial escape rate is decreased when the potential V drives molecules further into the chamber. So the small-t behavior of $f_1(t)$ for chitosan hexaose, and by assumption chitohexaose, is dominated by backward escape. Finally, since *Ec*ChiP can be expressed by *E. coli* when only chitosugars are available and its average binding characteristics $k_{\rm on}$ and τ_C are similar to those of other chitosugar transporters, it is likely that chitohexaose translocation proceeds with reasonable efficiency. Together this implies that translocation occurs, but only at large t, and that the translocation probability P_T is similar to the measurable parameter $\tilde{P}_T$.

The value of the transport current Q_T in Eq. (1) could be measured directly. If the sugar concentration on both sides of the membrane was measured as a function of t then the current could be obtained. (One would have to account for the affect of backflow occurring as the concentration on the two sides of the membrane approached equilibrium.) The sugar current Q_T through a single channel, which cannot exceed $k_{\rm on}[c]$, is limited to a few hundred molecules per second at a concentration of $[c] = 100\ \mu$M. Thus a viable measurement of Q_T would require a membrane perforated with a large number of channels that conduct sugar in parallel. Since the qualitative behavior of $f_1(t)$ is robust, the average of $f_1(t)$ over many channels would give the nonlinear curve and a measurable $\tilde{P}_T$. The results of this measurement could be used to obtain P_T and the claim that $\tilde{P}_T \approx P_T$ tested.

V. CONCLUSION

The current $I(t)$ through a single channel of *Ec*ChiP, a monomeric protein channel for chitosugars that is associated with a silent gene in *E. coli*, has been measured and analyzed. The measured probability $f_1(t)$ for a sugar molecule to remain trapped within the monomer beyond time t exhibits a distinctive t dependence, with an initial rapid decay followed by much slower decay. The initial decay is, based on its V dependence for charged chitosan hexaose, dominated by events in which the sugar escapes back to the side of the membrane from which it entered. The slow long-t escape rate λ_1 is independent of V and likely receives a contribution from successful translocation events, in which the molecule escapes to the opposite side of the membrane. We claim that a valuable estimate for the probability P_T that sugar is translocated through the membrane may be obtained from the measurable property $\tilde{P}_T$, the extrapolated intercept of the high-t behavior of $f_1(t)$.

These results emphasize the need to go beyond τ_C, which is often used as the only characteristic of escape dynamics, in the characterization of the transport channel. By studying the detailed t dependence of $f_1(t)$, for *Ec*ChiP, occurring when chitohexaose was replaced with chitopentaose or as a function of V, we were able to develop a phenomenological picture useful for connecting the $I(t)$ data with sugar transport.

ACKNOWLEDGMENTS

Funding was provided by Suranaree University of Technology and the Office of the Higher Education Commission under the NRU project of Thailand. H.S.M.S. was supported by Suranaree University of Technology through an SUT-OROG grant. This author's ten-month research visit in Germany was supported by the Deutscher Akademischer Austausch Dienst. W.S. acknowledges the Thailand Research Fund and Suranaree University of Technology through a Basic Research Grant (No. BRG578001) and an SUT grant (No. SUT1-102-60-36-13). W.M. was supported by a DPST scholarship provided by the Royal Government of Thailand. We thank the group of Professor Mathias Winterhalter at Jacobs University, Bremen, Germany for generously providing access to high-time-resolution BLM equipment and supplies.

H.S.M.S. and W.S. designed and performed single-channel BLM experiments. W.M. and M.F.S. performed data analysis and theoretical calculations. M.F.S. wrote the paper.

APPENDIX: RANDOM-WALK MODEL OF INTRAMONOMER DYNAMICS

There is a substantial amount of literature devoted to modeling OMP channels that utilize molecular dynamical simulations based on a realistic description of the channel structure and other techniques [5,6,48]. For our purposes, a phenomenological description of the monomer that illustrates the relationship between $f_1(t)$, P_T and $\tilde{P}_T$, in the simplest context, is sufficient. We model the monomer as a series of N trapping sites with sugar molecules undergoing 1D Brownian motion among these sites [49,50]. Trapping sites are labeled $\alpha = 0,1,2,\ldots,N-1$ from the *cis* end to the *trans* end (see Fig. 8). A sugar molecule that enters the channel from the *cis* chamber becomes bound in the zeroth site at time $t = 0$ and can hop from site to site. When any site is occupied, the ionic current is assumed to be $I(t) \approx I_1$.

At time $t > 0$, the probability of finding the molecule at site α is $g_\alpha(t)$, so $f_1(t) = \sum_\alpha g_\alpha(t)$. The rate for a molecule to hop from the α site to the $\alpha \pm 1$ site $\Lambda_\alpha^\pm$ is constant in time. Here Λ_0^- is the backward escape rate into the *cis* chamber that determines the initial slope, i.e., $\Lambda_0^- = -f_1'(0)$. A dimensionless time variable τ is defined by

$$\tau \equiv \Lambda_0^- t. \tag{A1}$$

Hopping rates are similarly expressed in units of Λ_0^- so $\Lambda_0^- \equiv 1$ and all $\Lambda_\alpha^\pm$ are dimensionless.

At time $\tau = 0$, the molecule is bound in the $\alpha = 0$ site, so $g_\alpha(0) = \delta_0^\alpha$. We solve $d\mathbf{g}/d\tau = \mathbf{\Lambda g}$, where $\mathbf{g}(\tau)$ is a vector with components $g_\alpha(\tau)$ and $\mathbf{\Lambda}$ is a matrix with all elements equal to zero except $\Lambda_{\alpha,\alpha} = -\Lambda_\alpha^+ - \Lambda_\alpha^-$ and $\Lambda_{\alpha,\alpha\pm1} = \Lambda_{\alpha\pm1}^\mp$. This gives $\mathbf{g}(\tau) = \exp(\mathbf{\Lambda}\tau)\mathbf{g}(0)$, where the exponential of the matrix is shorthand for the Taylor series $\exp(\mathbf{\Lambda}\tau) \equiv \mathbf{1} + \mathbf{\Lambda}\tau + \mathbf{\Lambda}\cdot\mathbf{\Lambda}\tau^2/2 + \cdots$, where $\mathbf{1}$ is the $N \times N$ unit matrix.

The behavior of $f_1(\tau)$ at small times, obtained from the first few terms of the Taylor series, is

$$-\ln f_1(\tau) \approx \tau - \Lambda_0^+\frac{\tau^2}{2} + \Lambda_0^+(\Lambda_0^+ + \Lambda_1^- - 1)\frac{\tau^3}{6} + \cdots \quad \text{(small } \tau\text{)}. \tag{A2}$$

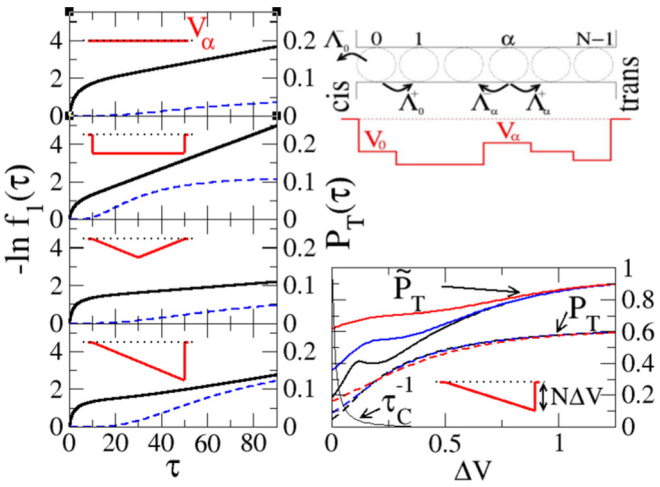

FIG. 8. Escape of a molecule from the channel, modeled as a 1D random walk. The top right shows the model monomer with N trapping sites $\alpha = 0,1,2,\ldots$ from *cis* to *trans* sides. A molecule hops at rate $\Lambda_\alpha^\pm$ from α to $\alpha \pm 1$ so $\Lambda_0^- = -f_1'(0)$ is the escape rate to the *cis* chamber. These $\Lambda_\alpha^\pm$ depend on effective potential V_α. Shown on the left are simulation results from the model for various effective potentials V_α (indicated in red and labeled in the top panel) and $N = 20$. The solid black curves show the logarithm of $f_1(\tau)$, the probability for the molecule to remain in the channel beyond time τ, where τ is the time variable. Dashed blue curves show the probability $P_T(\tau)$ for the molecule to be translocated from the *cis* to the *trans* side before time τ. The bottom right shows the wedge potential with steepness ΔV and probability $P_T = P_T(\infty)$ (dashed line) compared to $\tilde{P}_T$ (solid line) for $N = 20,10,5$ from bottom to top. The residence time τ_C in arbitrary units is shown for $N = 20$.

The first term in the series describes molecules that escape back to the *cis* chamber immediately after being trapped at $\alpha = 0$. The next few terms describe molecules that undertake short walks into the monomer before escaping back to the *cis* chamber. Translocation processes do not occur until the Nth-order term, which is negligible at small time τ.

More explicitly, the solution can be written $g_\alpha(\tau) = \sum_n u_{n,\alpha}u_{n,0}\exp(-\lambda_n\tau)$ with $f_1(\tau) = \sum_{n=1}^N p_n \exp(-\lambda_n\tau)$ and $p_n = (\Lambda_0^- u_{n,0} + \Lambda_{N-1}^+ u_{n,N-1})u_{n,0}\lambda_n^{-1}$, where each λ_n is an eigenvalue of $\mathbf{\Lambda}$ and $u_{n,\alpha}$ is the αth component of the corresponding eigenvector. These eigenvalues satisfy $\sum \lambda_n p_n = \Lambda_0^-$.

The simplest nontrivial version of this model has $N = 2$ trapping sites and two eigenvalues λ_n that are functions of the three independent hopping parameters. If applied to the $f_1(t)$ data above, one has to select hopping parameters with a large variation so that the slope of $\ln f_1(t)$ changes by orders of magnitude. Having done this, the calculated curve $\ln f_1(t)$ tends to exhibit a sharp elbow where the slope changes from a large value to a small value. It is difficult to reproduce the smooth evolution of the $\ln f_1(t)$ data with this model. We instead consider models with a much larger number of sites, which have the correct qualitative behavior. [If the hopping parameters are assumed to be equal, as in model (i) below, we can solve the above equations analytically for any N and thus gain some physical insight.]

At large times τ, the sum of exponentials is dominated by the term with the smallest positive eigenvalue, which we denote by λ_1. This gives

$$-\ln f_1(\tau) \approx B_0 + \lambda_1\tau + \cdots \quad (\text{large } \tau), \tag{A3}$$

with $\tilde{P}_T = \exp(-B_0) = p_1$. The probability of translocation $P_T(\tau)$ occurring before time τ is

$$P_T(\tau) = \int_0^\tau d\tau' g_{N-1}(\tau')\Lambda_{N-1}^+ \tag{A4}$$

with the total probability of translocation $P_T \equiv P_T(\infty)$. Both P_T and $\tilde{P}_T$ can be calculated and the claim that the measurable quantity $\tilde{P}_T$ is an approximation to the translocation probability P_T can be tested within the context of this model.

Sample calculations of $f_1(\tau)$ and $P_T(\tau)$, for an arbitrary channel size $N = 20$, are shown in the left panels of Fig. 8. The $\Lambda_\alpha^\pm$ values are written in terms of a dimensionless potential energy V_α, which binds the sugar molecule at each trapping site, according to $\Lambda_\alpha^\pm = \exp(V_\alpha - V_{\alpha\pm1})$ with zero potential outside the monomer. The V_α indicated in Fig. 8 are, from top to bottom, (i) $V_\alpha = 0$, giving all $\Lambda_\alpha^\pm = 1$, (ii) $V_\alpha = -1$, giving fast intramonomer hopping with slower escape at each end of the channel, (iii) a symmetric wedge potential with $V_\alpha = -0.1(\alpha + 1)$ for $\alpha < N/2$, and (iv) an asymmetric wedge potential $V_\alpha = -0.1(\alpha + 1)$ for all α.

The calculations of $f_1(\tau)$ have similar qualitative behavior to the data of Figs. 4 and 5. That is, the curve $\ln f_1(\tau)$ changes rapidly at small τ and then the slope approaches a constant with a much smaller value at large τ. The small-τ behavior is sensitive to the binding potential at the *cis* mouth. The final slope λ_1 is largely determined by the length of the channel, since propagation through a long channel is the rate-limiting mechanism. For the cases shown, $P_T(\tau)$ is negligible at small τ and does not start to increase appreciably until $f_1(\tau)$ is approaching its large-τ limit.

In the bottom right plot, P_T is compared to $\tilde{P}_T$ for the asymmetric wedge potential. They follow a similar trend with variation of the wedge steepness ΔV. At large ΔV, the descending linear potential gives a transmission probability P_T that approaches unity. The average time that the monomer remains blocked τ_C increases rapidly with ΔV.

The connection between $\tilde{P}_T$ and P_T is evident from the results above. Both $f_1(\tau)$ and P_T are given by sums over eigenvectors n. If we approximate each sum by the $n = 1$ term associated with the smallest eigenvalue then we find

$$\tilde{P}_T = (1/\lambda_1)\left(u_{1,0}^2\Lambda_0^- + u_{1,0}u_{1,N-1}\Lambda_{N-1}^+\right) \tag{A5}$$

and

$$P_T \approx (1/\lambda_1)u_{1,0}u_{1,N-1}\Lambda_{N-1}^+. \tag{A6}$$

The first term on the right-hand side of Eq. (A5) describes backward escape to the *cis* side during the large-τ regime. The second term, also appearing in Eq. (A6), describes large-τ translocation. An equality is established between $\tilde{P}_T$ and P_T by making two assumptions: (a) The second term in Eq. (A5) dominates over the first and (b) the sum over n that determines P_T is well approximated by its $n = 1$ term. The validity of these two assumption depends on V_α.

When $V_\alpha = 0$ and all hopping rates are equal to one, the equations above can be evaluated analytically. The eigenvalues

are

$$\lambda_n = 2 - 2\cos\left[\frac{n\pi}{N+1}\right], \tag{A7}$$

with $n = 1,2,\ldots,N+1$ varying over a range of order $1/N^2$ and producing a $f_1(t)$ function with the same qualitative behavior as the data when N is large. The weights p_n satisfy

$$p_n = \cos^2\left(\frac{n\pi}{2(N+1)}\right)[1-(-1)^n]. \tag{A8}$$

Further, the analytic results yield $P_T = 1/(N+1)$ and, assuming $N \gg 1$, $\tilde{P}_T = 4/(N+1)$. The two terms in Eq. (A5) are equal and the $n = 1$ term is twice as large as the full series giving P_T. Combining the errors in both assumptions, $\tilde{P}_T$ overestimates P_T by a factor of 4. For the remaining examples of the left-hand side of Fig. 8, $\tilde{P}_T$ overestimates P_T by factors 4, 2.6, and 2.2, respectively. The estimate becomes more accurate as the steepness of the asymmetric wedge potential ΔV increases.

Generally, $\tilde{P}_T$ gives the probability that a molecule is retained in the channel for a time much greater than required for initial backward escape. It does not tell us whether the molecule will be translocated. For effective potentials V_α that present large barriers to translocation, one finds $\tilde{P}_T \gg P_T$ and $P_T \ll 1$. For a channel designed to translocate sugar, one can suppose that translocation is not prevented by a large energy barrier. If this is the case, then reasonable values for V_α result in $\tilde{P}_T \gtrapprox P_T$ to within a factor of order unity.

[1] H. Nikaido, J. Bioenerg. Biomembr. **25**, 581 (1993).
[2] C. Andersen, M. Jordy, and R. Benz, J. Gen. Physiol. **105**, 385 (1995).
[3] C. Andersen, R. Cseh, K. Schüelein, and R. Benz, J. Membr. Biol. **164**, 263 (1998).
[4] S. M. Bezrukov, J. Memb. Biol. **174**, 1 (2000).
[5] H. Nikaido, Microbiol. Mol. Biol. Rev. **67**, 593 (2003).
[6] B. Roux, T. Allen, S. Berneche, and W. Im, Q. Rev. Biophys. **37**, 15 (2004).
[7] S. Szmelcman and M. Hofnung, J. Bacteriol. **124**, 112 (1975).
[8] E. G. Saravolac, N. F. Taylor, R. Benz, and R. R. Hancock, J. Bacteriol. **173**, 4970 (1991).
[9] K. Schulein, K. Schmid, and R. Benz, R. Mol. Microbiol. **5**, 2233 (1991).
[10] T. Schirmer, J. Struct. Biol. **121**, 101 (1998).
[11] R. Dutzler, Y.-F. Wang, P. J. Rizkallah, J. P. Rosenbusch, and T. Schirmer, Structure **4**, 127 (1996).
[12] Y.-F. Wang, R. Dutzler, P. J. RIzkallah, J. P. Rosenbusch, and T. Schirmer, J. Mol. Biol. **272**, 56 (1997).
[13] M. Watanabe, J. Rosenbusch, T. Schirmer, and M. Karplus, Biophys. J. **72**, 2094 (1997).
[14] T. Schirmer, T. A. Keller, Y. F. Wang, and J. P. Rosenbusch, Science **267**, 512 (1995).
[15] C. Hilty and M. Winterhalter, Phys. Rev. Lett. **86**, 5624 (2001).
[16] W. Im and B. Roux, J. Mol. Biol. **322**, 851 (2002).
[17] N. O. Keyhani, X. B. Li, and S. Roseman, J. Biol. Chem. **275**, 33068 (2000).
[18] N. O. Keyhani and S. Roseman, Biochim. Biophys. Acta **1473**, 108 (1999).
[19] X. Li and S. Roseman, Proc. Natl. Acad. Sci. U.S.A. **101**, 627 (2004).
[20] B. L. Bassler, C. Yu, Y. C. Lee, and S. Roseman, J. Biol. Chem. **266**, 24276 (1991).
[21] D. E. Hunt, D. Gevers, N. M. Vahora, and M. F. Polz, Appl. Env. Microbiol. **74**, 44 (2008).
[22] C. Pruzzo, L. Vezzulli, and R. R. Colwell, Env. Microbiol. **10**, 1400 (2008).
[23] K. K. Meibom, X. B. Li, A. T. Nielsen, C. Y. Wu, S. Roseman, and G. K. Schoolnik, Proc. Natl. Acad. Sci. U.S.A. **101**, 2524 (2004).
[24] W. Suginta, W. Chumjan, K. R. Mahendran, A. Schulte, and M. Winterhalter, J. Biol. Chem. **288**, 11038 (2013).
[25] W. Suginta, M. Winterhalter, and M. F. Smith, Biochim. Biophys. Acta **1858**, 3032 (2016).
[26] T. Mizuno, M. Y. Chou, and M. Inouye, Proc. Natl. Acad. Sci. U.S.A. **81**, 1966 (1984).
[27] M. Guillier, S. Gottesman, and G. Storz, Genes Dev. **20**, 2338 (2006).
[28] J. Vogel and K. Papenfort, Curr. Opin. Microbiol. **9**, 605 (2006).
[29] A. A. Rasmussen, J. Johansen, J. S. Nielsen, M. Overgaard, B. Kallipolitis, and P. A. Valentin-Hansen, Mol. Microbiol. **72**, 566 (2009).
[30] N. Figueroa-Bossi, M. Valentini, L. Malleret, F. Fiorini, and L. Bossi, Genes Dev. **23**, 2004 (2009).
[31] H. S. M. Soysa and W. Suginta, J. Biol. Chem. **291**, 13622 (2016).
[32] H. S. M. Soysa, A. Schulte, and W. Suginta, J. Biol. Chem. **292**, 19328 (2017).
[33] R. Benz, A. Schmid, and G. H. Vos-Scheperkeuter, J. Membr. Biol. **100**, 21 (1987).
[34] M. Winterhalter, Curr. Opin. Colloid Interface Sci. **5**, 250 (2000).
[35] E. Berkane, F. Orlik, A. Charbit, C. Danelon, D. Fournier, R. Benz, and M. Winterhalter, J. Nanobiotech. **3**, 3 (2005).
[36] L. Kullman, P. A. Gurnev, M. Winterhalter, and S. M. Bezrukov, Phys. Rev. Lett. **96**, 038101 (2006).
[37] W. Suginta, W. Chumjan, K. R. Mahendran, P. Janning, A. Schulte, and M. Winterhalter, PLoS One **8**, e55126 (2013).
[38] W. Suginta and M. F. Smith, Phys. Rev. Lett. **110**, 238102 (2013).
[39] M. Montal and P. Mueller, Proc. Natl. Acad. Sci. U.S.A. **69**, 3561 (1972).
[40] C. Danelon, T. Brando, and M. Winterhalter, J. Biol. Chem. **278**, 35542 (2003).
[41] G. Schwarz, C. Danelon, and M. Winterhalter, Biophys. J. **84**, 2990 (2003).
[42] http://swissmodel.expasy.org/
[43] S. Biswas, M. M. Mohammad, D. R. Patel, L. Movileanu, and B. van den Berg, Nat. Struct. Mol. Biol. **14**, 1108 (2007).
[44] www.pymol.org
[45] C. Andersen, B. Schiffler, A. Charbit, and R. Benz, J. Biol. Chem. **277**, 41318 (2002).
[46] L. Kullman, M. Winterhalter, and S. M. Bezrukov, Biophys. J. **82**, 803 (2002).
[47] C. Calero, J. Faraudo, and M. Aguilella-Arzo, Phys. Rev. E **83**, 021908 (2011).
[48] P. Hanggi and F. Marchesoni, Rev. Mod. Phys. **81**, 387 (2009).
[49] R. Phillips, J. Kondev, J. Theriot, and H. G. Garcia, *Physical Biology of the Cell* (Garland, New York, 2013).
[50] N. G. Van Kampen, *Stochastic Processes in Physics and Chemistry* (Elsevier, Amsterdam, 1992).